Pergamon

Journal of Structural Geology, Vol. 20, No. 2/3, pp. 163 to 173, 1998

0191-8141/98 $19.00 + 0.00

PII: S0191-8141(97)00074-6

Stress gradients around porphyroclasts: palaeopiezometric estimates and numerical modelling

T. KENKMANN and G. DRESEN

GeoForschungsZentrum Potsdam, Telegrafenberg, 14473 Potsdam, Germany

(*Received* 13 *December* 1996; *accepted in revised form* 10 *September* 1997)

Abstract—Based on strain gradients commonly found around porphyroclasts, the mechanical interaction of porphyroclasts and recrystallized mylonite matrix in a retrograde amphibolite-facies shear zone of the Ivrea–Verbano Zone, Italy, was investigated. Differential stresses inferred from recrystallized grain size and dislocation density indicate stress concentrations at the porphyroclast–matrix interface of about 1.7–2.0 with respect to the average in the matrix. The palaeopiezometric stress data are compared to the results of a finite-element model composed of two rheologically different phases. In this model, the local distribution and concentration of stresses around porphyroclasts mostly depend on clast–matrix coupling and the effective viscosity contrast of the two phases. The bulk strength and work hardening of the composite system increases with interface coupling. Both the modified stress field and the reduced average grain size around porphyroclasts may result locally in instabilities, and promote strain localization and a change in the dominant deformation mechanism. © 1998 Elsevier Science Ltd.

INTRODUCTION

Porphyroclasts are relatively rigid inclusions embedded in a fine-grained, ductile matrix which is commonly present in rocks deformed in ductile shear zones. They occur in a wide range of sizes and shapes, and correspond to relics of the undeformed protolith. Porphyroclasts affect the mechanical behaviour of a mylonite. As is well known for ceramics and metal composites, inclusions with a different strength to the matrix influence the bulk constitutive behaviour and may locally cause inhomogeneous plastic flow. Strain in the mylonitic matrix and flow around inclusions have been investigated both in analogue and theoretical models (Masuda and Ando, 1988; Ildefonse and Mancktelow, 1993; Bjørnerud and Zhang, 1994; Odonne, 1994; Ten Brink, 1996). Stress gradients around porphyroclasts may also enhance chemical reactions and diffusional mass transfer in the porphyroclast vicinity (Gresens, 1966). To investigate the effect of porphyroclasts in ductile deformation, estimates of the differential stress around these inclusions are required.

In this paper we focus on the partitioning of stress between porphyroclasts and the surrounding mylonitic matrix. In the first part of this study we show the typical microstructure of an amphibolite-facies shear zone (Fig. 1) around some hornblende and clinopyroxene porphyroclasts. In an attempt to investigate the mechanical effect of porphyroclasts on ductile deformation, we studied local changes of the microstructure. We observed gradients in the microstructure (recrystallized grain size, shape and dislocation density) that suggest the existence of gradients in flow stress. In the second part of the paper, we compare our microstructural data to the results of a finite-element model which is used to calculate the stress distribution around an inclusion stronger than the matrix in a two-phase material.

In the past, flow stresses around porphyroclasts were investigated by Strömgard (1973) and Masuda and Ando (1988) using different mathematical approaches. They consider the interface between porphyroclast and matrix to be fully coupled. The problem of interface bonding between matrix and porphyroclast as a function of matrix strain was recently studied by Ildefonse and Mancktelow (1993) and Odonne (1994) using analogue models. Odonne (1994) found that the degree of bonding has a greater effect on finite strain of the matrix than the viscosity ratio of the materials. Theoretically, two mechanisms of decoupling of porphyroclast and matrix are possible: opening of voids in the pressure shadows; or sliding along the interface. Porphyroclasts associated with pressure shadows give evidence for separation between the porphyroclast and the ductile matrix. But microstructural evidence for interface sliding between porphyroclast and matrix is more difficult to find.

Because of its possible importance in natural shear zones, we investigated the effect of interface coupling accompanied by the formation of pressure shadows on the flow stress distribution around an inclusion. We also varied the viscosity contrast between porphyroclast and matrix and the applied shear stress, which will also affect the stress distribution. A comparison of stress estimates based on palaeopiezometry and modelled stress distribution around an inclusion is used to discuss the importance of porphyroclasts in the deformation of fine-grained mylonites.

GEOLOGICAL SETTING AND PETROGRAPHIC DESCRIPTION

The samples were obtained from a mylonite zone of the Ivrea–Verbano Zone (IVZ), Italy. The IVZ is generally thought to represent a tilted segment of lower to intermediate continental crust forming the pre-Alpine

Fig. 1. Photomicrograph of the investigated high-temperature shear zone showing mylonite (MYL) and ultramylonite bands (UMYL). The ultramylonites consist of fine hornblende, plagioclase and ilmenite grains. Porphyroclasts within the mylonitic matrix are hornblende (HBL) and clinopyroxene (CPX) with opaque asymmetric pressure shadows indicating a top-to-the-left shear sense. The lower edge is 2 cm.

basement of the southern Alps (Brodie and Rutter, 1987; Rutter *et al.*, 1993). The IVZ consists of a succession of steeply dipping metamorphic rocks ranging from granulite to amphibolite facies. Its base is formed by layered igneous basic to ultrabasic intrusions, which are overlain by pyroxene gneisses, amphibolites and metapelites, with metamorphic grade continuously decreasing towards the top. For an introduction to the geology of the IVZ see, for example, Zingg (1983) and Rutter *et al.* (1993).

The investigated shear zone belongs to a network of amphibolite- to granulite-facies shear zones trending subparallel to the structural layering of the IVZ. These shear zones have been interpreted as low-angle extensional faults related to thinning and extension in the lower to middle crust during the Early Mesozoic (Brodie and Rutter, 1987; Brodie *et al.*, 1989). Deformation was active during and after the peak of regional metamorphism (Brodie *et al.*, 1989).

The shear zone chosen for this study is located approximately 1 km southeast of Finero (Val Cannobina) near the transition of hornblende peridotites of the Finero Complex to metagabbros of the mafic body. The protolith is a hornblende metagabbro containing plagioclase, hornblende, clinopyroxene, garnet, orthopyroxene and ilmenite. The evolution of the shear zone from the undeformed metagabbro to the fine-grained ultramylonites is discontinuous, and layers with different average grain size usually have sharp contacts. Here, we focus on the fine-grained ultramylonitic layers (grain size of 10–50 μm) of the shear zone (Fig. 1). In these domains the matrix grain size is about two orders of magnitude smaller than in the undeformed protolith.

The granulite-facies protolith (830°C $\pm$ 50°C and 860 MPa $\pm$ 50 MPa) experienced a metasomatism leading to the growth of garnet and hornblende at temperatures between 650 and 700°C and a maximum pressure of 750 MPa (Franz, personal communication), prior to the formation of the ultramylonites. The shear zone was then active under retrograde conditions ranging from 650 to 500°C and from 600 to 400 MPa (Kenkmann, 1997). A later greenschist-facies overprint occurs in parts of the shear zone, with the formation of epidote, sphene, actinolite, albite and chlorite.

The ultramylonite matrix consists mainly of plagioclase, hornblende, clinopyroxene and ilmenite (Fig. 2). Amphibole in the matrix is either an edenitic hornblende or a magnesio hornblende (for amphibole nomenclature see Leake, 1978). Plagioclase composition mainly varies from Ab_{50} to Ab_{75}. In the ultramylonites, the presence of intragranular fluid inclusions as well as the results of infrared spectrometry of the matrix minerals indicate that fluids were present during deformation (Kenkmann, 1997). Porphyroclasts within the ultramylonites are amphiboles and clinopyroxenes. Amphibole porphyroclasts are either ferroan pargasitic hornblende or tschermakitic hornblende (Kenkmann and Dresen, 1996). Clinopyroxene porphyroclasts are either diopsides or augites.

ANALYTICAL PROCEDURES

Microstructures were studied using both an optical microscope and a scanning electron microscope (Zeiss DSM 962) in backscattered-electron mode. Thin sections were cut parallel to the lineation (X) and normal to the foliation. To estimate the matrix grain size we assumed ellipsoidal grain shapes, and measured long and short axes of each grain. The average grain size is given as the diameter of a circle of the same area as the ellipsoid. The grain size mapping was performed measuring about 1000 grains at intersecting points of an equispaced grid. To determine the crystallographic texture of the ultramylonite we investigated four samples with a X-ray diffraction

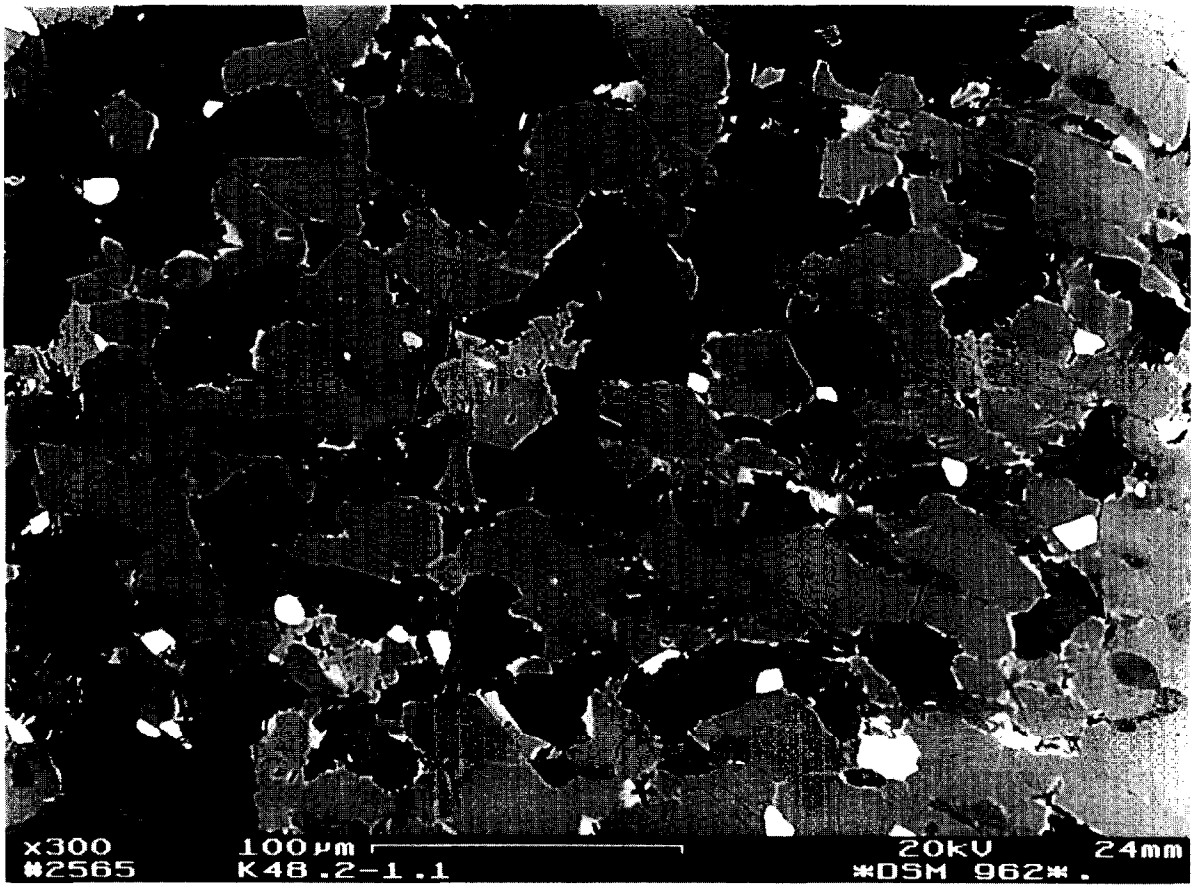

Fig. 2. Backscattered SEM image of the mylonitic matrix (X–Z section). Hornblende is grey, plagioclase is black and ilmenite is white. Hornblende forms an interconnected network of recrystallized grains. Hornblende grains show aspect ratios averaging $R_{xz} = 1.8$ and a shape-preferred orientation with long axes oriented 20–40° to the foliation forming an oblique foliation to the mylonitic foliation (horizontal). Near the rims hornblende is partly enriched in iron. Plagioclase grains are frequently isolated and have irregular shapes. Alteration product visible is chlorite (dark grey).

texture goniometer (Philips PW 1729). Specimens for transmission electron microscopy (TEM) were prepared from doubly polished sections using a Gatan ion mill. We used a Philips CM 200 twin microscope at 200 kV. To measure dislocation densities we used plates with magnifications of between 20,000 and 50,000, and determined the number of dislocation endpoints in the area of projection (Underwood, 1970). Using a tilt-rotation stage, we tried to obtain the highest possible diffraction contrast for each measurement with the maximum number of visible dislocations.

MICROSTRUCTURAL OBSERVATIONS

Mylonitic matrix

The microstructure of the mylonitic matrix is modified around the porphyroclasts. In cross-sections containing the foliation and its normal we can define four quadrants around the porphyroclasts, which differ with respect to matrix grain size and grain shape. Generally, two opposite quadrants with reduced matrix grain size and high aspect ratio alternate with two quadrants where grain size is larger than average and grain aspect ratios are low (Fig. 3). This indicates a relatively fast equilibration of the microstructure in the matrix close to the porphyroclasts compared to the displacement rates. This was found qualitatively around both hornblende and clinopyroxene porphyroclasts and irrespective of their aspect ratios. Maximum and minimum matrix grain size was determined around several porphyroclasts. Figure 4 shows the typical variation of matrix grain size around one porphyroclast analysed in detail. The systematic change in microstructure was used to infer differential stress gradients in the mylonitic matrix around the porphyroclasts.

The mylonite matrix consists dominantly of amphibole (55 vol.%), plagioclase (37 vol.%) and ilmenite (8 vol.%). The mylonitic foliation of the shear zone is defined by a layering in mineralogical composition and grain size (Fig. 1). Hornblende commonly forms an interconnected network of grains with average aspect ratios of 1.8, showing a shape-preferred orientation with the long axes oriented 20–40° to the mylonitic foliation (Figs 2 & 3). It also exhibits a strong crystallographic-

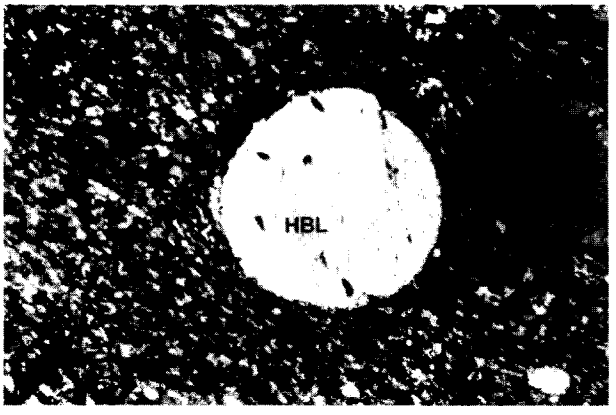

Fig. 3. Spherical hornblende porphyroclast from an ultramylonite band (X–Z section, crossed nicols). The porphyroclast diameter is 650 μm top to bottom (scale bar: 125 μm). Within the recrystallized matrix, hornblende shows gradients in grain size and aspect ratio. A finer grain size and increased aspect ratios dominates in the lower-left and upper-right quadrants near the porphyroclast. Larger, more equant, grains can be found in the upper-left and lower-right near the pressure shadows. The pressure shadows are filled with opaque ilmenite.

preferred orientation with [110] forming a girdle normal to the X-direction (Kenkmann, 1997), which may be related to (100)[001] slip (Skrotzki, 1990). Undulose extinction and subgrain boundaries occur frequently. Our TEM observations show that free dislocations in hornblende are dominantly straight and long. Loops with long straight segments parallel to [001] are common. Additionally, planar defects of variable width bounded by partial dislocations also occur. Dislocations are often arranged in regular dislocation arrays that define low-angle subgrain boundaries. This suggests that amphibole recrystallizes dynamically via subgrain rotation. (We use the term 'dynamic recrystallization' in the sense of Urai *et al.* (1986) who included geochemical changes during recrystallization.) Additionally, we also observed microfracturing parallel to {110} and nucleation of new amphiboles within plagioclase grains.

Plagioclase frequently fills isolated pockets surrounded by hornblende. A crystallographic-preferred orientation is only weakly developed. An [020] girdle normal to the lineation may indicate (010)[001] and/or (010)[100] slip (Ji and Mainprice, 1988). Plagioclase is sometimes twinned (pericline and albite law). Subgrains are very rare. We found nucleation and growth (neocrystallization) of plagioclase within amphiboles. In the recrystallized and neocrystallized grains, the albite content seems to increase with decreasing grain size. In areas of reduced matrix grain size around the porphyroclast the albite content locally increases from Ab_{57} up to Ab_{90} (Kenkmann, 1997).

Porphyroclasts

Within the ultramylonites most hornblende and clinopyroxene porphyroclasts are ellipsoidal (aspect ratio $R_{xz} > 2$) or almost spherical ($R < 1.3$), 500–2000 μm in diameter (Fig. 1). The spherical shape of the porphyroclasts (Fig. 3) may arise from rolling during non-coaxial flow of the matrix. This is also suggested by a random distribution of [001] and [100] of spherical clinopyroxene porphyroclasts, which would be expected from rolling and mechanical abrasion. Recrystallized mantles and tails, such as those commonly observed in quartz or feldspar porphyroclasts of granitic mylonites, are absent in these rocks. However, most of the hornblende and clinopyroxene porphyroclasts show well-developed, asymmetrical pressure shadows filled with massive ilmenite. The filled pressure shadows indicate that diffusive mass transfer plays an important role in the deformation of the mylonites. TEM observations on clinopyroxene porphyroclasts show an increasing number of twin-lamellae towards the surface of the porphyroclast. In the clinopyroxene and hornblende porphyroclasts we also found low-angle grain boundaries more frequently close to the interface.

PALAEOPIEZOMETRY

In a crystalline solid, the density of free dislocations is related to the applied stress (Bird *et al.*, 1969; Kohlstedt and Weathers, 1980; De Bresser, 1996). Previous work has also shown that, during steady-state deformation, the dynamically recrystallized grain size depends on the magnitude of the applied differential stress (Twiss, 1977; Ross *et al.*, 1980; Gleason and Tullis, 1993). We assume that the microstructure reflects steady-state conditions as there are no indicators for a significant static overprint. Previous studies have mostly focused on quartz palaeopiezometry to estimate palaeostresses in shear zones (Kohlstedt and Weathers, 1980; Ord and Christie, 1984). In this study we use recrystallized grain size in hornblende, and dislocation density in hornblende and plagioclase, as palaeopiezometers.

Recrystallized grain size

Twiss (1977) empirically showed that the dynamically recrystallized grain size D is inversely related to differential stress $\Delta\sigma$. This may be expressed by the equation (Skrotzki, 1992):

$$\Delta\sigma = \mu(D/(20b))^{-0.75}, \quad (1)$$

where b is the Burger's vector ($b_{HBL} = [001] = 0.533$ nm) and μ is the shear modulus ($\mu_{HBL} = 50$ GPa) of hornblende. Figure 4 and Table 1 present the results for hornblende in the vicinity of the porphyroclast. The average grain size in the mylonitic matrix is 24.8 μm for hornblende. Near the porphyroclast the hornblende grain size varies between 42 and 12 μm. Two maxima and minima can be distinguished around the porphyroclast. The grain size minima contain two subminima. The grain size maxima near the pressure shadows are elongated into the foliation plane and are asymmetrically

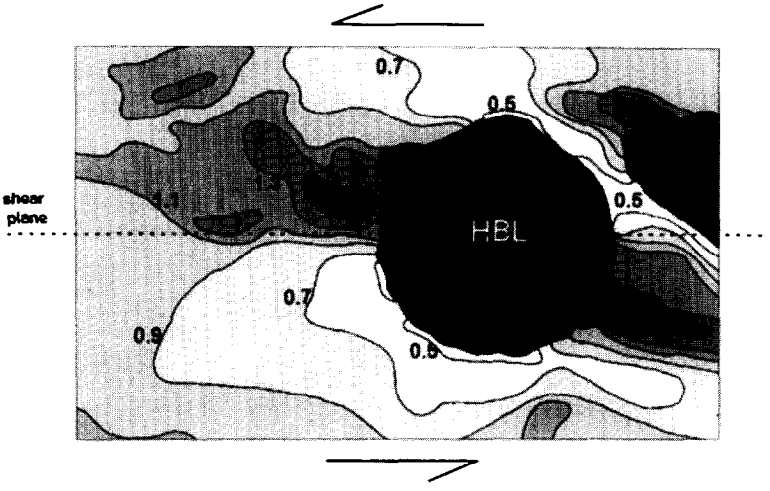

Fig. 4. Grain size distribution of hornblende matrix grains around the hornblende porphyroclast of Fig. 3. Contours are normalized for the average matrix grain size ($D/D_{average}$). Two minima and maxima are visible. The minima split into two small subminima at the porphyroclast–matrix interface. Normalized grain size spans from 1.5 close to the pressure shadows to 0.5 in the opposite quadrants (see Table 1).

Table 1. Grain size D of recrystallized hornblende and the normalized grain size $D/D_{average}$. $\Delta\sigma$ is the estimated differential stress based on D. $\Delta\sigma/\Delta\sigma_{average}$ is normalized to the average stress in the matrix. Magnitudes are valid for the isolines of the contour plot in Fig. 4

Grain size D (μm)	$D/D_{average}$	$\Delta\sigma$ (MPa)	$\Delta\sigma/\Delta\sigma_{average}$
12.4	0.5	251	1.7
17.4	0.7	195	1.3
22.4	0.9	161	1.1
24.8	1	150	1
27.4	1.1	139	0.9
32.4	1.3	122	0.8
37.4	1.5	110	0.7

distributed with respect to the pressure shadows. Using equation (1) we determined differential stresses from 100 MPa up to 260 MPa in the fine-grained domains around the porphyroclast in Fig. 4. Average flow stress in the matrix is 150 MPa based on hornblende grain size (Table 1). As no experimental calibration for hornblende has so far been performed, we use the normalized flow stress C to indicate the stress distribution around the porphyroclasts, where:

$$C_{max} = \Delta\sigma_{max}\text{interface}/\Delta\sigma_{average}\text{matrix} \quad (2)$$

$$C_{min} = \Delta\sigma_{min}\text{interface}/\Delta\sigma_{average}\text{matrix}. \quad (3)$$

Using the data of Fig. 4, the normalized flow stresses are $C_{max} = 1.7$ and $C_{min} = 0.65$.

Dislocation density

The relation between dislocation density and differential stress is based on elastic theory (Taylor, 1934), and was successfully applied to metals, alloys and silicates, such as quartz and olivine. Differential stress $\Delta\sigma$ as a function of dislocation density ρ is given by an equation of the form (e.g. Kohlstedt and Weathers, 1980):

$$\Delta\sigma = \mu\alpha b\rho^{0.5} \quad (4)$$

where μ is the shear modulus ($\mu_{Plag} = 40$ GPa, $\mu_{HBL} = 50$ GPa), α is a numerical factor ranging from 1 to 3, and b is the Burger's vector ($b_{Plag} = [001] = 0.71$ nm, $b_{HBL} = [001] = 0.533$ nm). Again, stresses are normalized with respect to the average matrix stress, as α is not known for hornblende or plagioclase. Densities of free dislocations of both hornblende and plagioclase grains in the matrix were measured around four porphyroclasts. The average dislocation density in plagioclase (1.5×10^9 cm^{-2}) is lower than in hornblende (3×10^9 cm^{-2}). The dislocation density increases significantly by about one order of magnitude to 1.5×10^{10}–2×10^{10} cm^{-2} at the matrix–clast interface for both plagioclase and hornblende. Dislocation density starts to increase abruptly at a distance of less than 0.2 of the porphyroclast radius (Fig. 5a) and is highest close to the porphyroclast–matrix interface. Close to the pressure shadows, the dislocation density is slightly lower compared to the matrix (Fig. 5b). The normalized flow stresses are $C_{max} = 2.0$ and $C_{min} = 0.8$. Both values inferred from dislocation densities are higher than from recrystallized grain size. We conclude that changes in dislocation density and grain size reflect an important perturbation of the stress field around porphyroclasts, and a pronounced stress concentration at the porphyroclast–matrix interface.

NUMERICAL MODELLING OF THE STRESS DISTRIBUTION IN A COMPOSITE SYSTEM

The finite-element model

In an attempt to correlate our palaeopiezometric data

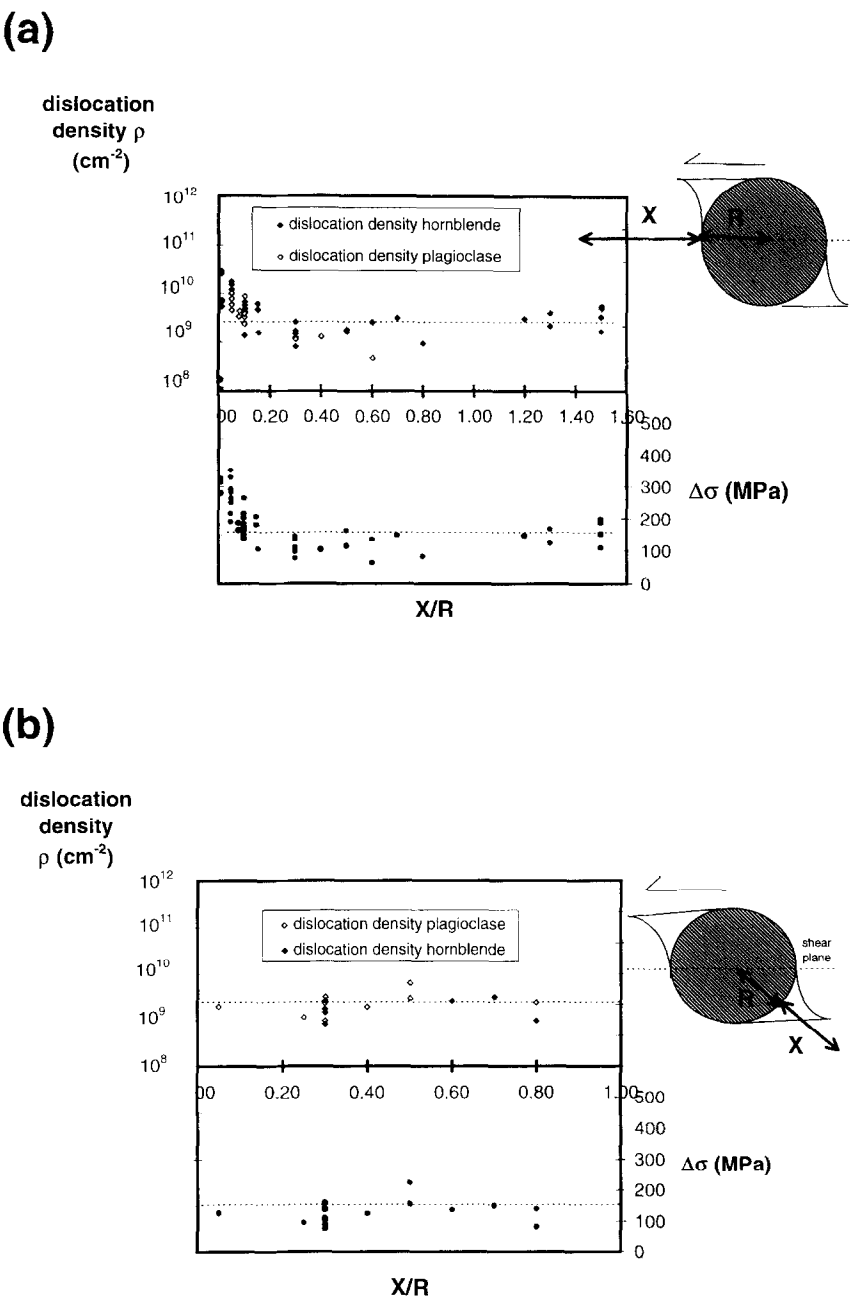

Fig. 5. Dislocation density profiles and estimated differential stresses with respect to the relative distance from the porphyroclast. The dotted lines represent the average dislocation density in hornblende and flow stress, respectively. (a) Profile along the foliation towards the porphyroclast–matrix interface. Dislocation density abruptly increases at a distance of 0.2 of the clast radius. (b) Dislocation densities and estimated flow stresses in a profile along the x-direction of finite strain.

to the stress distribution around porphyroclasts we have used a commercial finite-element (FE) package (MARC Analysis Research Corporation 1994). This numerical model permits one to study the stress distribution in a two-phase matrix–inclusion system deforming in power-law creep.

The model is based on a two-dimensional quadrilateral plane-strain finite-element mesh consisting of 540 elements and 601 nodes (Fig. 6). A mesh refinement towards the central inclusion was required for better resolution of the heterogeneous stress field at the inclusion–matrix interface. The model width is eight times the inclusion diameter (Fig. 6). A power-law creep equation of the form:

$$\dot{\epsilon} = A\Delta\sigma^{n}\exp(-Q/RT) \tag{5}$$

was used to model the steady-state flow of porphyroclast and matrix material, where $\dot{\epsilon}$ is the axial strain rate, A is the pre-exponential factor, $\Delta\sigma$ is the differential stress, n is the stress exponent, Q is the activation enthalpy, R is the gas constant and T is the temperature. Constitutive equations for matrix and inclusion are from Caristan (1982) and Boland and Tullis (1986), respectively (Table 2). For all calculations we assumed a temperature of

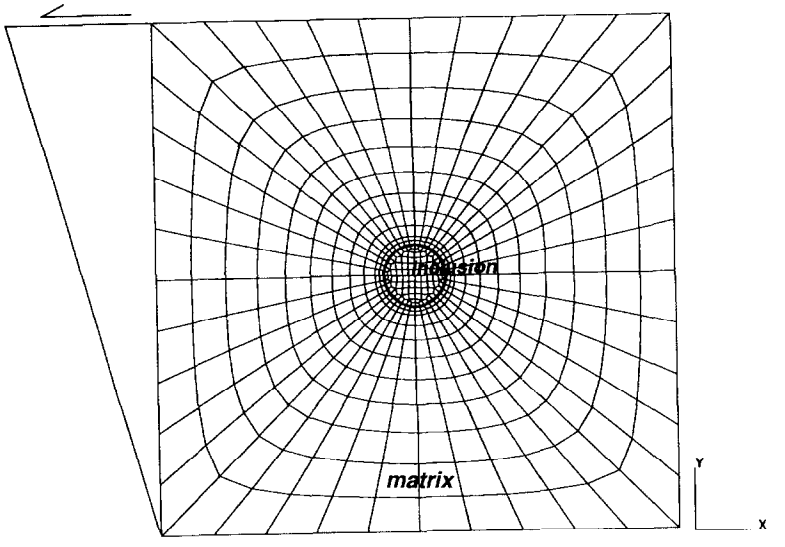

Fig. 6. Finite-element grid used in the numerical model. The sphere in the centre contains 100 elements and is modelled with a different rheology from the surrounding matrix. Inclusion and matrix do not share common nodes. The boundary conditions are: lower edge remains fixed; nodes on left, right and top side can only be displaced in the x-direction. A shear stress is applied on the top side in the x-direction.

700°C (Table 2). Axial strain was converted to plane strain using a factor of $0.5 \times 3^{[(n+1)/2]}$ (Tullis *et al.*, 1991; Chester, 1995). We varied the matrix rheology to achieve different viscosity contrasts between inclusion and matrix. The effective viscosity η_{eff} and the effective viscosity contrast r are given as:

$$\eta_{\text{eff}} = 0.5\Delta\sigma/\dot{\epsilon} \tag{6}$$

$$r = \log(\eta_{\text{eff}}\text{clast}/\eta_{\text{eff}}\text{matrix}). \tag{7}$$

The model was deformed in simple shear and at constant load. Stresses of 10, 25 and 50 MPa were applied to the upper edge of the model. The nodes at the bottom remained fixed and the nodes on vertical edges were allowed to move in the x-direction only. Because of a large distortion of the element mesh during simple shear, leading to numerical problems, remeshing is required at a shear strain of $\gamma = 1.0$–1.5.

Inclusion and matrix elements do not share common nodes. We investigated variable degrees of coupling of the inclusion and the matrix. Cohesive friction (or constant shear friction) along the interface is defined by the expression:

$$f_t \leq -mt\Delta\sigma/\sqrt{3}, \tag{8}$$

where f_t is the tangential force being applied, m is the friction factor, $\Delta\sigma$ is the flow stress of the material being deformed and t is the tangent unit vector in the direction of relative movement. Changing the friction factor m or the relative sliding velocity, we vary the tolerated amount of sliding along the interface. The degree of coupling is expressed by slip distance along the interface referred to circumference of the inclusion in percent. This value ranges from 0.0% (completely coupled) to about 10% (uncoupled). In addition, gap opening occurs if a given tensile force normal to the interface is exceeded. These gaps are suggested to represent pressure shadows of natural porphyroclasts.

Model results

We focus on three parameters that affect the flow stress distribution surrounding an inclusion: (1) interface

Table 2. Material properties used in the finite-element model

	Clast	Matrix
Elastic properties		
Young's modulus	167 000 MPa	100 100 MPa
Poisson's ratio	0.25	0.31
	Levien *et al.* (1979)	Kern and Richter (1981)
Plastic properties		
Flow law for dislocation creep:	$n = 3.3$,	$n = 3.05$,
$\dot{\epsilon} = A\Delta\sigma^n \exp(-Q/RT)$	$\log A = 5.17$ MPa^{-n} s^{-1},	$\log A = -1.2$ MPa^{-n} s^{-1},
Correction for plane strain:	$Q = 490$ kJ mol^{-1},	$Q = 276$ kJ mol^{-1},
$0.5 \times 3^{[(n+1)/2]}$	$T = 700$°C	$T = 700$°C
	Boland and Tullis (1986)	Caristan (1982)

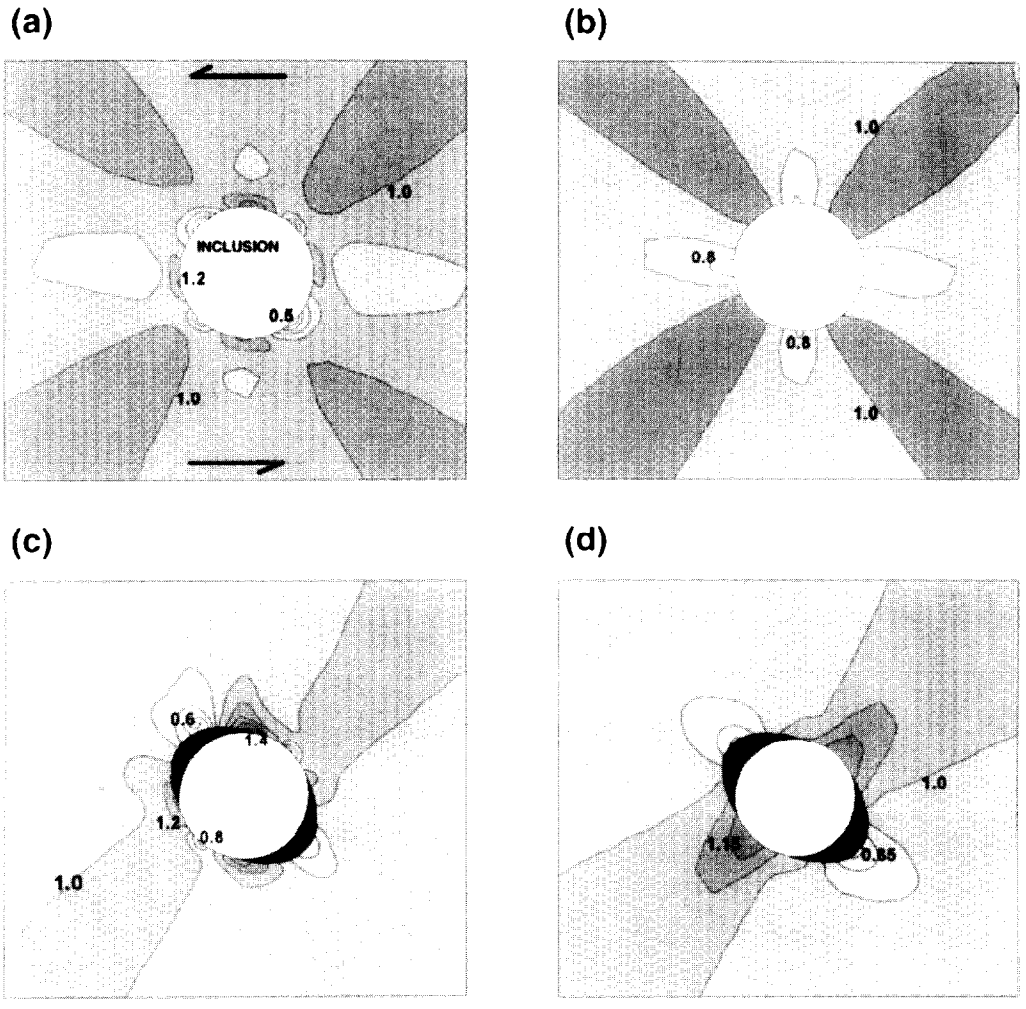

Fig. 7. Differential stress distributions around a spherical inclusion obtained with the numerical model under different interface conditions. Differential stress is normalized to the stress of a reference node. The shear strain γ is 0.45 ± 0.03. (a) No gap opening, no interface sliding. (b) No gap opening, interface sliding. (c) Gap opening, no interface sliding. (d) Gap opening, interface sliding.

coupling and gap opening between inclusion and matrix; (2) the effective viscosity ratio between inclusion and matrix; and (3) the applied shear stress.

(1) If the interface between the inclusion and matrix is fully coupled, the stress field near the interface shows four local maxima, which are shifted by 45° to the maxima of the far-field stress (Fig. 7a). This stress distribution is comparable to the results presented by Masuda and Ando (1988). The stress magnitude is largest at the interface on both the x- and y-axes. These maxima disappear if interface sliding is introduced (Fig. 7b). The symmetry of the stress field changes if gaps are allowed to open between the matrix and the inclusion. Only two maxima and minima remain at the interface (Fig. 7c & d). The flow stress maxima are split into two submaxima if interface sliding is suppressed (Fig. 7c).

(2) Increasing the viscosity contrast of inclusion and matrix also increases the stress concentration in the matrix, provided that the matrix and inclusion are coupled (Fig. 8). If there is no coupling and interface sliding is strong ($> 1\%$), then increasing the viscosity

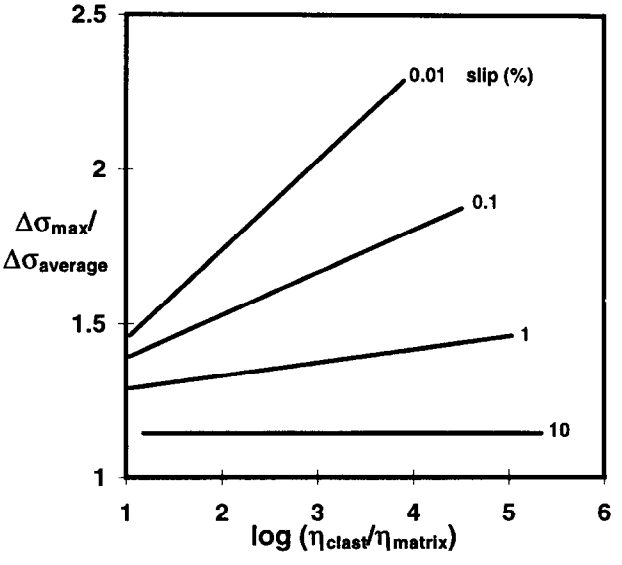

Fig. 8. Diagram showing the dependence of the stress concentration C_{max} on the viscosity contrast between matrix and inclusion for gap opening and different degrees of interface sliding. Slip at the interface normalized to the circumference of the inclusion is used to indicate the degree of interface coupling. This value ranges from 0% (completely coupled) to about 10% (uncoupled).

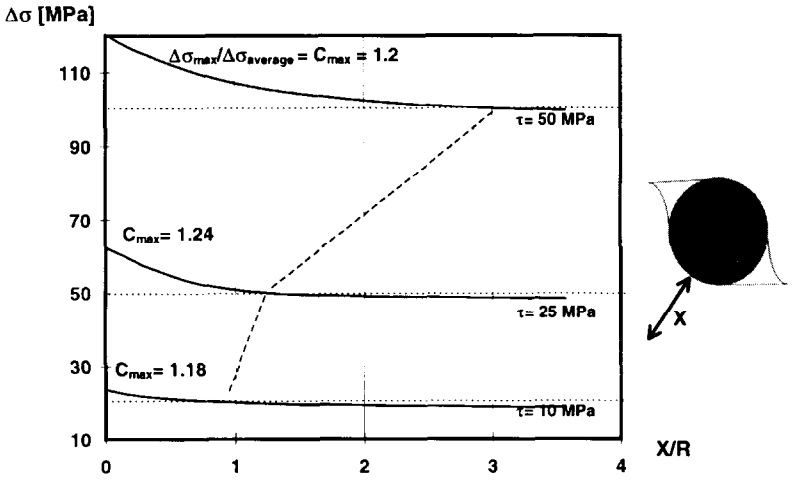

Fig. 9. Flow stress traverses oriented 45° to the x-axis of the model. The local stress concentration remains roughly unchanged with $C_{max} \approx 1.2$ for different applied shear stresses. (Conditions: gap opening, ~4% interface sliding, material properties of inclusion and matrix given in Table 2, shear strain $\gamma = 0.57 \pm 0.03$.)

contrast has almost no effect on the stress concentration.

(3) In Fig. 9 we show the variation of shear stress along traverses oriented 45° to the x-axis of the model for different shear stresses. The local stress concentration remains roughly unchanged with $C_{max} = 1.2$ for given boundary conditions. However, the extent of the stress concentrations into the matrix strongly depends on the applied shear stress. With applied shear stresses increasing from 10 to 50 MPa the width of the maxima increases from one inclusion radius to three. The width also depends on C_{max} which, in turn, depends on the viscosity contrast and coupling.

DISCUSSION

Application to mylonites

There is no experimental calibration of hornblende and plagioclase palaeopiezometers based on recrystallized grain size or dislocation density. This may be the main reason for the discrepancy between the flow stresses calculated with these two different methods. Also, calibrations of palaeopiezometers are always given for monomineralic aggregates. The mutual influence of different minerals in polymineralic rocks on the relation between stress and microstructure is not well understood (White, 1979; Kohlstedt and Weathers, 1980). It is also possible that static recovery may affect recrystallized grain size and dislocation densities in different ways. Furthermore, the storage of dislocations may continue under lower temperature conditions, where recovery and recrystallization are less active (White, 1979). Prior *et al.* (1990) pointed out that the rate of microstructural changes and the cooling history of a rock have a strong influence on the conservation of the microstructure. Therefore, we restrict our discussion to the normalized stresses rather than absolute values.

In the ultramylonite, the maximum stress concentration around the investigated porphyroclasts, C_{max}, inferred from recrystallized grain size and dislocation density, varied between 1.7 and about 2.0, respectively. In the numerical model C_{max} varied between 1.05 and 2.3 for a wide range of boundary conditions including the magnitude of flow stress, coupling across the interface and viscosity contrast between the inclusion and matrix.

The modelling suggests that the stress distribution in the matrix depends on the degree of interface coupling (Fig. 7). Thus, the pattern of recrystallized grain size and dislocation densities around porphyroclasts should also depend on the porphyroclast–matrix coupling. The investigated porphyroclast of Fig. 3 shows two local minima and maxima in grain size (Fig. 4). Compared with the stress distribution in the finite-element model (Fig. 7), this observation suggests a partial separation of porphyroclasts and matrix, and the formation of pressure shadows. In fact, all of the observed porphyroclasts show pressure shadows, which are filled with precipitated ilmenite (Fig. 1). The grain size contours around the detailed analysed porphyroclast (Fig. 4) show that the grain size minimum is subdivided into two local subminima. These subminima are also observed in the model when gaps are allowed to form, but interface sliding between inclusion and matrix is small (Fig. 7c). Consequently, this may be an indication for reduced interface sliding.

The results of our model suggest that the stress concentration, C, at the interface depends mostly on the interface coupling (Fig. 7) and the viscosity contrast (Fig. 8). Strong stress and strain gradients result from strong inclusion–matrix coupling and/or a high viscosity ratio of the inclusion and matrix. Therefore, we interpret the strong gradient in dislocation density observed close to the investigated porphyroclasts (Fig. 5a) as indicative of a high viscosity contrast and/or limited interface sliding, associated with the separation of porphyroclast and matrix in the pressure shadows.

Localization of deformation

The presence of relatively rigid inclusions in a weaker material commonly increases the strength of the aggregate (Jordan, 1988; Tullis *et al.*, 1991; Dresen *et al.*, 1993). Figure 10 shows the effect of the interfacial coupling behaviour on the bulk strength in our model. The creep curves of the two-phase model with coupled interfaces show stronger work hardening compared to the pure material or the decoupled two-phase model (Fig. 10). Sliding along the interface and opening of tensile voids in the pressure shadows may lead to a pressure sensitivity of the aggregate and contribute to a transient mechanical response. In the investigated ultramylonites, decoupling of phases with different strengths may be facilitated by solution–precipitation processes and the local redeposition of material in pressure shadows (ilmenite).

Stress and strain gradients in the ultramylonites around relatively rigid porphyroclasts lead to a local reduction in recrystallized grain size (Figs 3 & 4). In these areas grain-size-sensitive diffusion processes and grain-boundary sliding may contribute more efficiently to deformation. However, in the presence of dislocation activity (Fig. 5a), microstructural evidence for diffusion creep is difficult to find. In fact, in the investigated mylonites of the Ivrea Zone we found that the dislocation density in both hornblende and plagioclase increases with decreasing matrix grain size.

Near the pressure shadows the differential stress is lower. Our estimate, based on recrystallized grain size and dislocation density, is 0.65–0.8 of the average flow stress in the matrix. This local stress minimum may lead to locally reduced strain and strain rate as indicated by low aspect ratios of the matrix grains in these areas (Fig. 3). Potentially, this stress drop and strain rate drop also affect the deformation behaviour of the matrix.

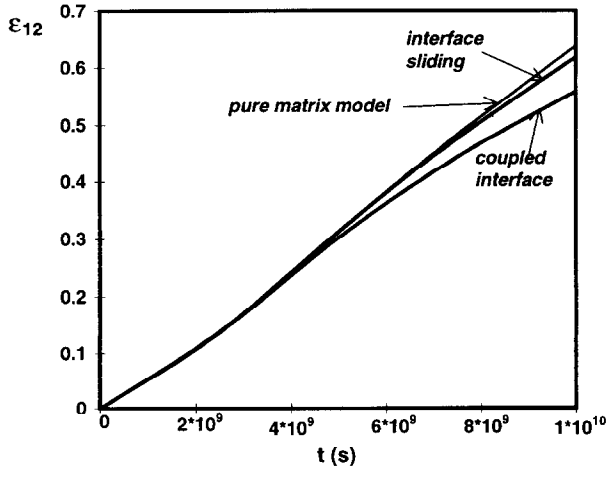

Fig. 10. Shear strain vs time. With interface sliding, the bulk creep rate of the composite is slightly lower than the pure matrix model. Full interface coupling leads to an increase in bulk strength and work hardening for the same material.

CONCLUSIONS

The following conclusions can be drawn regarding the stress distribution around porphyroclasts in mylonitic rocks.

(1) Magnitudes of stress concentration in the matrix close to porphyroclasts increase with the viscosity contrast and the degree of coupling between porphyroclast and matrix. Twice the average flow stress of the mylonitic matrix may not be exceeded where porphyroclasts are not interacting in the investigated shear zone.

(2) Inclusions affect the bulk strength of the aggregate and the work hardening rate; both increasing with interface coupling.

(3) Around the porphyroclasts, perturbations of grain size and stress potentially promote a change in the dominant deformation mechanism, leading to further localization of strain.

Acknowledgements T. Kenkmann gratefully acknowledges support by the GeoForschungsZentrum Potsdam. We sincerely thank R. Wirth for his help with the TEM and A. Zang for discussions of the FE model. K. Paech and S. Gehrmann carefully prepared ultrathin sections and TEM foils. We would like to thank J. Hippertt and A. McCaig for their review and critical comments which greatly helped to improve this paper.

REFERENCES

Bird, J. E., Mukherjee, A. K. and Dorn, J. F. (1969) Correlations between high temperature creep behavior and structure. In *Quantitative Relation Between Properties and Microstructure*, eds D. G. Brandon and R. Rosen, pp. 255–342. Israel Universities Press, Jerusalem.

Bjørnerud, M. G. and Zhang, H. (1994) Rotation of porphyroblasts in non-coaxial deformation: insights from computer simulations. *Journal of Metamorphic Geology* **12**, 135–139.

Boland, J. N. and Tullis, T. E. (1986) Deformation behavior of wet and dry clinopyroxenite in the brittle to ductile transition region. *American Geophysical Union Geophysical Monograph* **36**, 35–50.

Brodie, K. H., Rex, D. and Rutter, E. H. (1989) On the age of deep crustal extensional faulting in the Ivrea zone, northern Italy. In *Alpine Tectonics*, eds M. P. Coward, D. Dietrich and R. G. Park, pp. 203–210. Geological Society of London Special Publication **45**.

Brodie, K. H. and Rutter, E. H. (1987) Deep crustal extensional faulting in the Ivrea Zone of Northern Italy. *Tectonophysics* **140**, 193–212.

Caristan, Y. (1982) The transition from high-temperature creep to fracture in Maryland diabase. *Journal of Geophysical Research* **87**, 6781–6790.

Chester, F. M. (1995) A rheologic model for wet crust applied to strike-slip faults. *Journal of Geophysical Research* **100**, 13033–13044.

De Bresser, J. H. P. (1996) Steady state dislocation densities in experimentally deformed calcite materials: Single crystals versus polycrystals. *Journal of Geophysical Research* **101**, 22189–22201.

Dresen, G., Eckhardt, M., Evans, B. and Olgaard, D. (1993) Dispersion hardening in the fine-grained synthetic marbles. *EOS, Transactions of the American Geophysical Union* **74**, 590.

Gleason, G. C. and Tullis, J. (1993) Improving flow laws and piezometers for quartz and feldspar aggregates. *Geophysical Research Letters* **20**, 2111–2114.

Gresens, R. L. (1966) The effect of structurally produced pressure gradients on diffusion in rocks. *Journal of Geology* **74**, 307–321.

Ildefonse, B. and Mancktelow, N. S. (1993) Deformation around rigid particles: the influence of slip at the particle/matrix interface. *Tectonophysics* **221**, 345–359.

Ji, S. and Mainprice, D. (1988) Natural deformation fabrics of

plagioclase: implications for slip systems and seismic anisotropy. *Tectonophysics* **147**, 145–163.

Jordan, P. (1988) The rheology of polymineralic rocks—an approach. *Geologische Rundschau* **77**, 285–294.

Kenkmann, T. (1997) Verformungslokalisation in gabbroiden Gesteinen—mikrostrukturelle und mineralogische Untersuchungen in einer Hochtemperatur-Scherzone der Ivrea-Zone, Italien. Ph.D. thesis. Scientific Technical Report STR 97/12, GeoForschungszentrum Potsdam, 141 pp.

Kenkmann, T. and Dresen, G. (1996) The effect of porphyroclasts in deformation of fine-grained mylonites. In *Structure and Properties of High Strain Zones in Rocks, Verbania, Italy*, eds B. K. Brodie, E. H. Rutter, A. Boriani and L. Burlini. *Ricerca Scientifica ed Educazione Permanente, Supplemento* 107, 39.

Kern, H. and Richter, A. E. (1981) Temperature derivates of compressional and shear velocities in crustal and mantle rocks at 6 kbar confining pressure. *Journal of Geophysics* **49**, 47–56.

Kohlstedt, D. L. and Weathers, M. S. (1980) Deformation-induced microstructures, paleopiezometers, and differential stresses in deeply eroded fault zones. *Journal of Geophysical Research* **85**, 6269–6285.

Leake, B. E. (1978) Nomenclature of amphiboles. *Journal of the Mineralogical Association of Canada* **16**, 501–520.

Levien, L., Weidner, D. J. and Prewitt, C. T. (1979) Elasticity of diopside. *Physics and Chemistry of Minerals* **4**, 105–113.

Masuda, T. and Ando, S. (1988) Viscous flow around a rigid spherical body: a hydrodynamical approach. *Tectonophysics* **148**, 337–346.

Odonne, F. (1994) Kinematic behaviour of an interface and competence contrast: analogue models with different degrees of bonding between deformable inclusions and their matrix. *Journal of Structural Geology* **16**, 997–1006.

Ord, A. and Christie, J. M. (1984) Flow stresses from microstructures in mylonitic quarzites of the Moine Thrust zone. Assynt area, Scotland. *Journal of Structural Geology* **6**, 639–654.

Prior, D. J., Knipe, R. J. and Handy, M. R. (1990) Estimates of the rates of microstructural changes in mylonites. In *Deformation Mechanisms, Rheology and Tectonics*, eds R. J. Knipe and E. H. Rutter, pp. 309–319. Geological Society of London Special Publication **54**.

Ross, J. V., Ave Lallemant, H. G. and Carter, N. L. (1980) Stress dependance of recrystallized-grain and subgrain size in olivine. *Tectonophysics* **70**, 39–61.

Rutter, E. H., Brodie, K. H. and Evans, P. (1993) Structural geometry, lower crustal magmatic underplating and lithospheric stretching in the Ivrea zone, Northern Italy. *Journal of Structural Geology* **15**, 647–662.

Skrotzki, W. (1990) Microstructure in hornblende of a mylonitic amphibolite. In *Deformation Mechanisms, Rheology and Tectonics*, eds R. J. Knipe and E. H. Rutter, pp. 321–325. Geological Society of London Special Publication **54**.

Skrotzki, W. (1992) The geological significance of microstructural analyses by transmission electron microscopy. *Geotektonische Forschungen* **78**, 1–53.

Strömgard, K. E. (1973) Stress distribution during formation of boudinage and pressure shadows. *Tectonophysics* **16**, 215–248.

Taylor, G. I. (1934) The mechanisms of plastic deformation in crystals. *Proceedings of the Royal Society of London* **A145**, 362–404.

Ten Brink, C. E. (1996) Development of porphyroclast geometries during non-coaxial flow. An experimental and analytical investigation. Ph.D thesis, University of Utrecht. *Geologica Ultraiectina* **142**, 163 p.

Tullis, T. E., Horowitz, F. G. and Tullis, J. (1991) Flow laws of polyphase aggregates from end-member flow laws. *Journal of Geophysical Research* **96**, 8081–8096.

Twiss, R. J. (1977) Theory and applicability of a recrystallized grain size paleopiezometer. *Pure and Applied Geophysics* **115**, 227–244.

Underwood, E. E. (1970) *Quantitative Stereology*. Addison-Wesley, Reading, Massachusetts.

Urai, J. L., Means, W. D. and Lister, G. S. (1986) Dynamic recrystallization of minerals. *American Geophysical Union Geophysical Monograph* **36**, 161–199.

White, S. (1979) Difficulties associated with paleo-stress estimates. *Bulletin of Mineralogy* **102**, 210–215.

Zingg, A. (1983) The Ivrea and Strona–Ceneri zones (Southern Alps, Ticino and N-Italy)—A review. *Schweizerische mineralogische und petrographische Mitteilungen* **63**, 361–392.